J. Fluid Mech. (2000), *vol.* 414, *pp.* 75–103. Printed in the United Kingdom

An experimental investigation of higher-harmonic wave forces on a vertical cylinder

By MORTEN HUSEBY AND JOHN GRUE

Mechanics Division, Department of Mathematics, University of Oslo, Blindern, N-0316, Norway

(Received 24 May 1999 and in revised form 13 January 2000)

First- and higher-harmonic wave loads on a vertical circular cylinder are investigated experimentally in a wave tank of small scale. The incoming waves are (periodic) Stokes waves with wave slope up to 0.24. A large set of waves which are long compared to the cylinder radius is calibrated. The first seven harmonic components of the measured horizontal force on the cylinder are analysed. The higher-harmonic forces are significantly smaller than the first-harmonic force for all wave parameters. The measurements are continued until the wave amplitude is comparable to the cylinder radius, where the second-, third- and fourth-harmonic forces become of comparable size. Comparison with existing perturbation and fully nonlinear models shows, with a few exceptions, an overall good agreement for small and moderate wave amplitude. A fully nonlinear model agrees with the experiments even up to the seventh-harmonic force for part of the amplitude range. For the large amplitudes the models mostly give conservative predictions. It is important that the distance from the wave maker to the cylinder is large in order to avoid parasitic effects in the incoming wave field. The limited width of the wave tank is not important to the results except when close to resonance.

1. Introduction

Tension-leg and gravity-based platforms constructed from vertical cylinders may have a resonance period of up to a few seconds. These platforms may in high sea states experience responses of considerable amplitude that are very suddenly generated at the resonance period of the platform. This is a concern with respect to extreme loading. The generation of such responses, so-called 'ringing', is characterized by a resonant build-up during a time interval of the order one wave period. The wave period when this occurs may be several seconds, typically about 15 s. This is several times longer than the resonance period of the platform. The generation mechanism of the higher-harmonic wave loads leading to ringing of offshore structures is not yet well understood.

In recent times several attempts have been made to analyse this problem. The investigations are both theoretical and experimental. On the theoretical side, perturbation methods have been developed under the assumption of incoming Stokes waves. The objective has been to capture the wave loads up to the third-harmonic component (Faltinsen, Newman & Vinje 1995; Malenica & Molin 1995; Newman 1996*a*). Fully nonlinear methods have also been developed to analyse this problem (Cai & Melum 1996; Ferrant 1998). Several model tests and small-scale experiments have been undertaken, primarily on focused waves or irregular waves (Grue, Bjørshol & Strand 1993; Stansberg *et al.* 1995; Chaplin, Rainey & Yemm 1997).

To check the soundness and the domain of validity of the best numerical calculation methods for ringing analysis, it may be desirable to have available a set of experimental force measurements on periodic waves. A direct comparison of the first few harmonic force components can then be performed. This is the motivation of the present investigation. Small-scale experiments are undertaken with the purpose of measuring the horizontal higher-harmonic wave loads on a slender vertical circular cylinder in a wave tank. A relatively large range of wave amplitudes is investigated for waves which are long relative to the cylinder radius.

We have chosen to work with incoming Stokes waves in deep water. This corresponds to the assumptions in the perturbation methods. Moreover, the velocity field of the incoming waves has only one frequency, up to a relatively large wave slope. The higher-harmonic wave forces are then caused by the presence of the cylinder in the waves. We have put much effort into documenting the incoming wave field at the positions in the wave tank where the force measurements are carried out. The incoming waves become periodic, after a transient leading part, and for a time are not disturbed by parasitic waves. We carry out the force measurements in this period of time. At a later time, second-harmonic parasitic waves appear in the wave field. Our measurements of these waves agree with those of previous investigations, e.g. Schäffer (1996).

When the calibration of the incoming waves is finished, one of the two cylinders which are used in the experiments is mounted in the tank. The force measurements are carried out at a position 10 to 20 wavelengths from the wave maker. Since the incoming waves are long relative to the cylinder radius, the first-harmonic diffracted wave field is small. The higher-harmonic diffracted waves are quite visible, on the other hand.

As mentioned above, the force measurements are performed when the wave motion at the cylinder has become periodic. We shall find that the first-harmonic force always dominates the higher-harmonic forces. The latter are, however, of significant size, and we are able to analyse the complex force components up to the seventh harmonic. We compare the force measurements with available theoretical results, primarily for the first- second- and third-harmonic forces. The fully nonlinear model by Ferrant (1998) can, however, produce results for any of the harmonic forces. We compare our measurements with his computations and find rather good agreement up to the seventh-harmonic force, for part of the wave amplitude range of the experiments.

The ratio of the width of the wave tank to the cylinder diameter is 6–8 in this investigation. We find that the limited width of the wave tank is not important to the results, however, except when close to resonance. This means that a comparison between the experiments and the theoretical models is relevant, even though in the latter case the effect of tank walls is not included. During the course of the work we have found that the distance from the wave maker to the cylinder should be great, in order to avoid parasitic effects in the incoming wave field.

The paper is organized as follows. Following this Introduction, the experimental set-up is described in § 2. The incoming wave field is described and documented in § 3. The analysis of the force measurements and comparisons with theoretical models and other relevant experiments are presented in § 4. In § 5 certain oscillations of the force with respect to the wave slope are discussed. The oscillations are due to (unwanted) parasitic effects of the incoming wave field, which take place either when the recordings are performed in a late time window, or when the cylinder is too close to the wave maker. The effects of viscosity and separation are also commented on in § 5. Finally, § 6 is a conclusion.

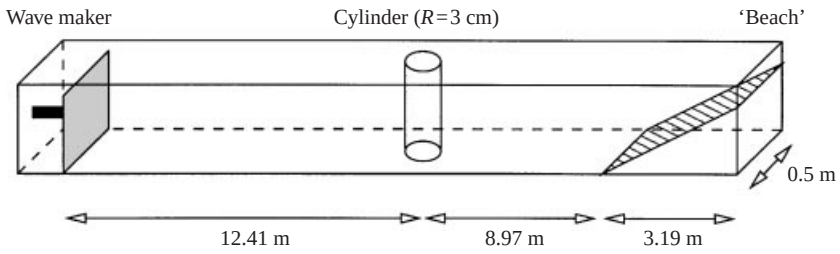

FIGURE 1. The wave tank for the case when the small cylinder is placed 12.41 m from the wave maker.

2. Experimental set-up

The measurements are carried out in a wave tank which is 24.6 m long, 0.5 m wide and filled with water to a depth of 0.6 m. At one end of the tank there is a wave maker consisting of a vertical plate (see figure 1). For controlling and monitoring the wave maker, and to record the surface elevation and the forces on the cylinder, we have used a computer with the data acquisition cards AT-MIO-16E-1 and AT-MIO-64E-3 from National Instruments. The update rate of the wave maker, and the sampling rate of the data acquisition, is 1000 Hz. At the opposite end of the wave tank there is an absorbing beach which reflects less than 3% of the amplitude of the incoming waves. The measurements are, however, taken before any small reflected waves at the fundamental frequency arrive at the cylinder. The motion of the wave maker is sinusoidal with constant amplitude, apart from a short initial period of 1 s, when the amplitude function rises from zero to the value of 0.99. The amplitude function has the form of a tanh-function. The generated wave train has a leading transient part, but is otherwise periodic, to a good approximation. First we calibrate the waves without the cylinder present in the wave tank. There are no measurements of wave elevation with the cylinder present.

We use standard resistance-type wire probes with Churchill amplifiers, to record the wave elevation. The wire probes have a nonlinearity of less than 1%. The amplifiers are calibrated statically at an accuracy of 0.25%. During the time of the experiments, we experience a drift of up to 1.5% out of calibration. The homogeneity of the water is an important factor in reducing the drift in the calibration. The amplifiers have also been tested using dynamic calibration. For different frequencies the error in the calibration ranges from –0.5% to +1.6%. Due to the somewhat random nature of these errors, we have not attempted to use any kind of transfer function in the analysis of the data. The reported wave amplitudes thus result from the Fourier transform of the pure data from the wave elevation amplifiers. Thus the errors in the measurements of wave elevation may in the worst case be about 4%. However, the actual relative error is believed to be smaller.

Two different cylinders are used in the experiments. One has radius $R = 3$ cm and the other has radius $R = 4$ cm. Both cylinders extend through the entire water depth. The resonance period of the cylinder in this set-up is measured to be 25 Hz. The cylinder is mounted rigidly to the wave tank by two force transducers, one at the bottom and one on top of the cylinder (figure 2).

The force transducers that have been used are Hottinger Baldwin Messtechnik Type Z6C2. We measure force in the longitudinal direction of the wave tank, and refer to the sum of the recorded forces as the force F. The force measurements are analysed by taking the Fourier transform over 10 wave periods, to evaluate the first

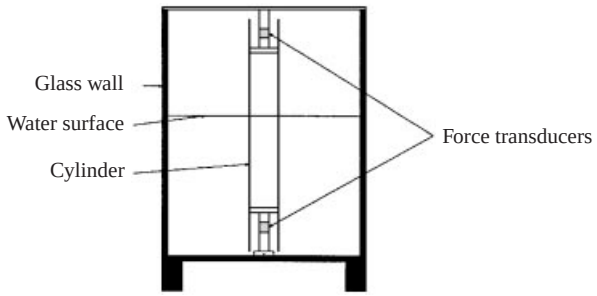

FIGURE 2. The wave tank in the plane orthogonal to the length of the tank.

seven harmonic components of F, i.e.

$$F = Re(F_1 e^{i\omega t} + F_2 e^{i2\omega t} \cdots + F_7 e^{i7\omega t} + \cdots), \tag{2.1}$$

where ω is the angular frequency of the waves and t is the time.

The first-harmonic wave amplitude A in the experiments, and the wavenumber k, are varied such that the wave slope Ak is between 0.05 and 0.24. The ratio A/R is between 0.13 and 1.14. The cylinder is placed at four different positions in the wave tank, at a distance from the wave maker varying from 6.33 m to 15.45 m. We measure the wave elevation at each of these four positions, at the exact position of the centre of the cylinder (which is mounted in the wave tank when the wave calibrations are finished). We also measure the wave elevation at 10 sub-positions within about one wavelength of the main position.

3. The wave input

As already noted, the incoming waves are measured at various positions, time windows, frequencies and amplitudes. For each cylinder we have chosen four different frequencies for the waves, giving a total of eight. Several of the frequencies are chosen so that we excite both cylinders with waves of the same non-dimensional wavenumber (table 1). In the table, T denotes the wave period, $f = 1/T$, and $\lambda = 2\pi/k$ denotes the wavelength.

For one frequency, $f = 1.425$ Hz, we have performed an extended series of measurements at four main positions and at 10 sub-positions around each main position, so that the waves are measured at 40 positions at a distance from the wave maker which is between 6 and 16 m. The purpose is to study how the waves develop as they propagate down the wave tank.

We primarily present force measurements for the small cylinder 12.41 m from the wave maker, and for the large cylinder 15.41 m from the wave maker. For each, the incoming waves are measured at 10 sub-positions, for 16 different amplitudes per wave frequency, giving a total of 1280 measurements of the incoming waves. The wave field is examined at different times after the start-up of the wave maker.

3.1. *How to avoid the parasitic waves*

A common problem in this type of experiment is the so-called parasitic waves, i.e. the free second-harmonic waves which originate at the wave maker. Here we circumvent this problem by taking the measurements before the parasitic waves have reached the cylinder. Below we show experimentally that the parasitic waves are absent for a

	$R = 3$ cm				$R = 4$ cm			
$f = 1/T$ (Hz)	1.171	1.300	1.425	1.615	1.009	1.123	1.399	1.532
λ (m)	1.14	0.92	0.77	0.60	1.51	1.23	0.80	0.67
$\max(A/R)$	1.145	0.931	0.776	0.603	1.145	0.931	0.603	0.503
kR	0.166	0.204	0.245	0.315	0.166	0.204	0.315	0.378

TABLE 1. Parameters for the incoming waves onto the cylinders of radius $R = 3$ and 4 cm. Wavelengths and wavenumbers are calculated for the linear case.

relatively large portion of the time of an individual measurement. We take all of the force measurements in this time window.

We measure the components of the second-harmonic wave elevation as explained in Grue (1992). We assume that the second-harmonic component of the waves $\eta^{(2)}(x,t)$ is of the form

$$\eta^{(2)}(x,t) = a_l^{(2)} \cos(2(kx - \omega t)) + a_f^{(2)} \cos(k_2 x - 2\omega(t - t_0)), \tag{3.1}$$

where ω and k satisfy the dispersion relation $\omega^2 = gk(1 + O(A^2k^2)) \tanh kh$, 2ω and k_2 satisfy $(2\omega)^2 = gk_2 \tanh k_2 h$, and where g is the acceleration due to gravity. Furthermore $a_l^{(2)}$ is the amplitude of the locked second-harmonic Stokes wave, $a_f^{(2)}$ is the amplitude of the free second-harmonic wave, t_0 determines the phase of the free wave relative to the locked wave, and x is the distance to the wave maker. For all wave parameters in the present investigation, we have $\omega^2 \approx gk(1 + A^2k^2)$ and $4\omega^2 \approx gk_2$, which means in practice that the waves are deep water waves.

The second-harmonic Fourier component of the wave elevation is obtained by

$$\hat{\eta}^{(2)}(x) = \frac{1}{10T} \int_0^{10T} \eta^{(2)}(x,t) \mathrm{e}^{-\mathrm{i}2\omega t} \, \mathrm{d}t. \tag{3.2}$$

By measuring $\hat{\eta}^{(2)}(x)$ at two positions, x_1 and $x_1 + \Delta x$, we obtain the amplitudes of the individual components of the second-harmonic wave elevation for a time interval of 10 wave periods. We then have (Grue 1992, equations 12 and 13)

$$a_l^{(2)} = \frac{1}{|\sin(k\Delta x)|} |\hat{\eta}^{(2)}(x_1) - \mathrm{e}^{\mathrm{i}4k\Delta x} \hat{\eta}^{(2)}(x_1 + \Delta x)|, \tag{3.3}$$

$$a_f^{(2)} = \frac{1}{|\sin(k\Delta x)|} |\hat{\eta}^{(2)}(x_1) - \mathrm{e}^{\mathrm{i}2k\Delta x} \hat{\eta}^{(2)}(x_1 + \Delta x)|. \tag{3.4}$$

Since the parasitic waves travel at half the speed of the main waves, they take twice as long to arrive at the cylinder as the leading part of the wave train. We thus have a time window where the parasitic waves have not yet reached the cylinder, there are no reflections from the beach, and the waves have become reasonably periodic. We have found that this time window begins at about 10–15 wave periods after the leading part of the wave train has reached the cylinder. An illustration of the time histories of the wave elevation and the corresponding force on the cylinder is provided in figure 3, where the actual time window (of reasonably periodic waves) is $35.088\,\mathrm{s} < t < 42.105\,\mathrm{s}$ (10 wave periods). In this time window we get a very small amplitude of the free second-harmonic wave elevation for wave slopes up to 0.2, indicating that parasitic waves are not present, see figure 4(*a*). Parasitic waves are present in a later time window, however, as we see in figure 4(*b*). The amplitude of

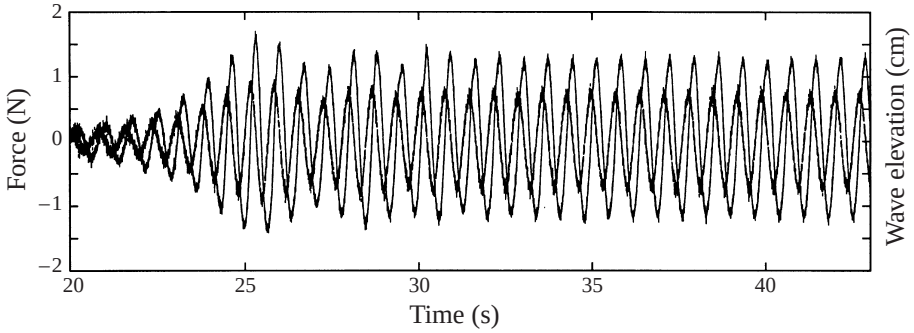

FIGURE 3. The time history of the wave elevation and the force on the small cylinder 12.41 m from the wave maker. In this case the time window we are using for the force measurements is from 35.088 s to 42.105 s, i.e. 10 wave periods. The curve with the greater amplitude represents the wave elevation. Here f =1.425 Hz and $Ak = 0.10$

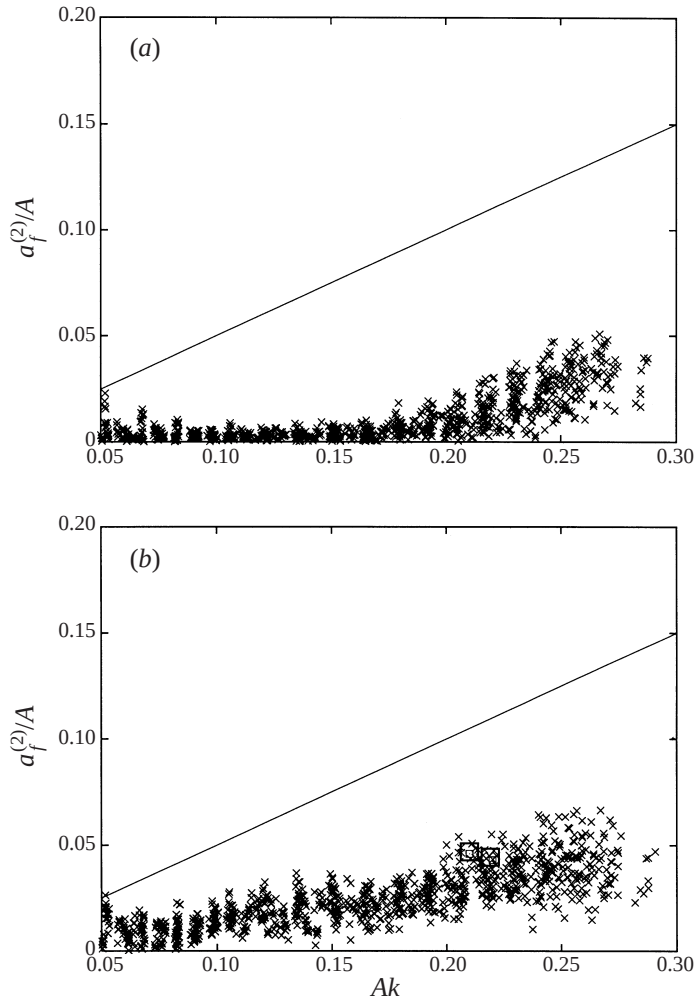

FIGURE 4. 1280 measurements (crosses) of free second-harmonic waves (parasitic waves) for f = 1.009, 1.123, 1.171, 1.300, 1.399, 1.425, 1.532, 1.615 Hz. Stokes theory (solid line) for the second-harmonic locked wave, $\frac{1}{2}A^2k$. Data (squares) due to Schäffer (1996). (*a*) Early time window. (*b*) Late time window.

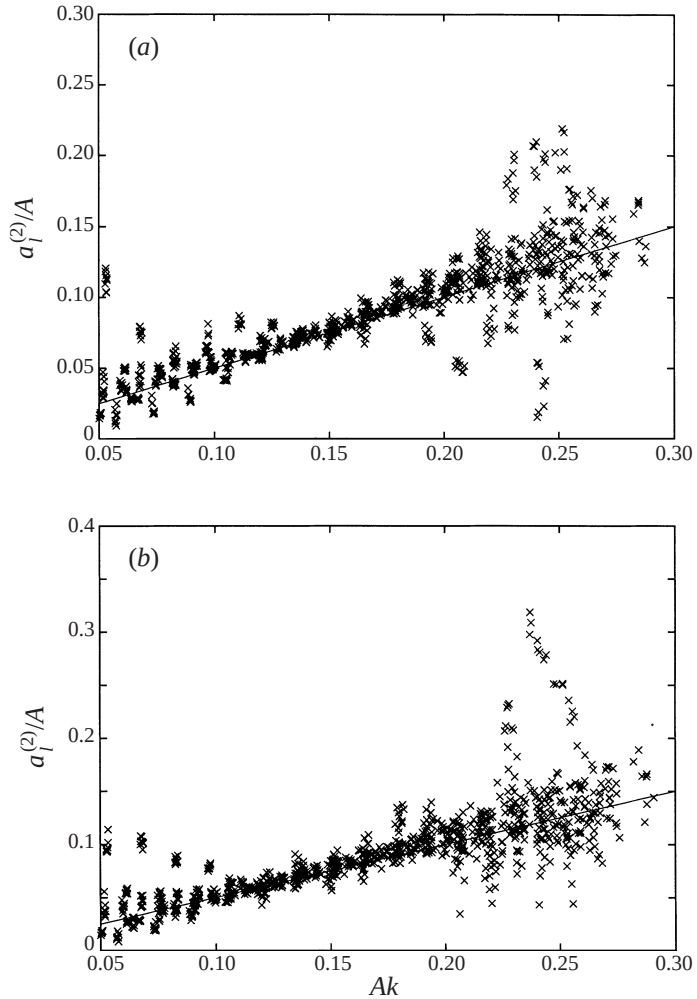

FIGURE 5. 1280 measurements (crosses) of locked second-harmonic waves for $f = 1.009$, 1.123, 1.171, 1.300, 1.399, 1.425, 1.532, 1.615 Hz. Stokes theory (solid line) for the second-harmonic locked wave, $\frac{1}{2}A^2k$. (*a*) Early time window. (*b*) Late time window.

the parasitic waves is about $\frac{1}{3}$ of the amplitude of the second-harmonic locked wave, i.e. $a_f^{(2)} \approx a_l^{(2)}/3 \approx 1/6A^2k$. After the parasitic waves have reached the cylinder, their amplitude is reasonably constant in time. In Schäffer (1996), the parasitic waves are calculated and measured in a set-up approximately similar to ours, for frequencies 1 Hz and 1.25 Hz, and wave slope of about 0.21. We see in figure 4(*b*) that our extensive measurements of the parasitic waves are in good agreement with Schäffer's results.

The locked second-harmonic Stokes waves are in reasonable agreement with Stokes theory (figure 5) for wave slopes up to 0.2, both before and after the parasitic waves have arrived at the position of the measurements. This means that $a_l^{(2)} \approx \frac{1}{2}A^2k$. We see that we have some experimental scatter at low wave slopes in our measurements. This is due to the fact that the amplitude of the waves is very small. Further details of the incoming wave field and how to accurately obtain the Fourier transform of the various time histories are described in the Appendices A and B.

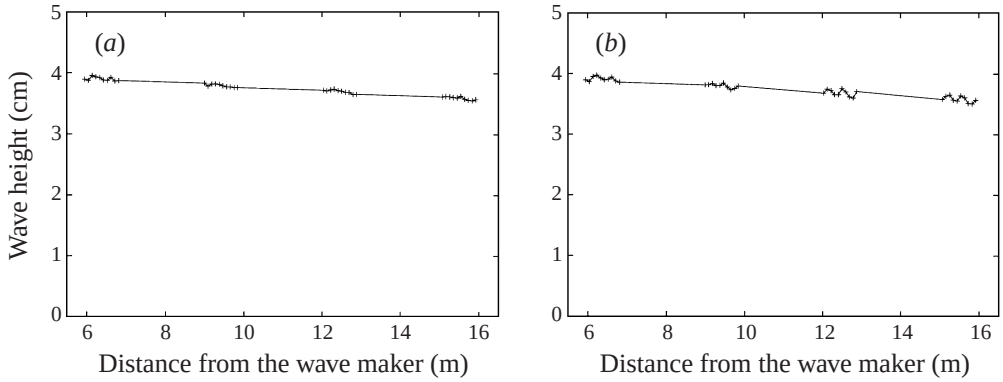

FIGURE 6. Wave height ($\eta_{max} - \eta_{min}$) at 40 different positions. Parameters: $Ak = 0.15$, $f = 1.425$ Hz. (a) Before and (b) after the parasitic waves have reached the cylinder.

In these experiments we could have employed a second-order wave maker theory to cancel out the parasitic waves. Third- and higher-harmonic free waves would still be present in the incoming waves, and would possibly affect the measurements of the third- and higher-harmonic forces. Since we take the measurements before the second- and higher-harmonic free waves reach the cylinder, such waves do not affect the measurements.

For further illustration of non-existence of the parasitic waves, we also show the wave elevation at 30 new positions (a total of 40) in the wave tank, for waves of frequency $f = 1.425$ Hz, in order to study how the waves develop as they propagate along the wave tank. The absence of parasitic waves is seen in figure 6, for the case of a wave with wave slope 0.15. In a time window before the parasitic waves have arrived at the measuring position, the waves propagate along the tank without any large oscillations in the wave height (figure 6a). When we choose a time window after the parasitic waves have reached the measuring position, we get oscillations of the wave height as we move further down in the wave tank (figure 6b). We note that the oscillations at the position closest to the wave maker in figure 6(a) are due to the fact that it is impossible to find a long enough time window (with periodic waves) where the parasitic waves have not reached the measuring position.

We observe that the amplitude of the waves decreases as a result of viscosity, by about 0.6% per wavelength. The frequency of the waves is measured to be exactly the same at all of the 40 measuring positions along the wave tank.

From these extensive measurements we can conclude that force measurements may be carried out in a reasonably long time window, where the incoming waves are quite periodic. The surface elevation may be regarded as close to pure Stokes waves up to $Ak \approx 0.2$, i.e.

$$\eta(t) = A\cos(kx - \omega t) + a_l^{(2)}\cos(2(kx - \omega t)) + a_l^{(3)}\cos(3(kx - \omega t)) + \cdots, \qquad (3.5)$$

where $a_l^{(2)} \approx (1/2)A^2k$ and $a_l^{(3)} \approx (3/8)A^3k^2$, according to Stokes theory. This also indicates that the incoming waves are represented by the velocity potential

$$\phi = Re\left[\frac{Ag}{i\omega}e^{ky}e^{i(kx-\omega t)}\right] + O(A^4), \qquad (3.6)$$

which determines the corresponding velocity and pressure fields. Here $\omega^2 = gk(1 + A^2k^2)$ and y denotes the vertical coordinate with $y = 0$ at the initially calm free surface.

4. The force

The first seven harmonic components of the force are presented. For all wavenumbers but one, we present measurements for wave slopes up to 0.2, since this is the range for which we know the wave input. For higher wave slopes when the waves can no longer be considered to be known, the force measurements will not have much value since there is no information on what causes the forces. However, for the wavenumber of $kR = 0.245$, we present measurements for wave slopes up to 0.24, to show the trend in the force as the wavenumber becomes greater, even though the force at these large wave slopes cannot be directly connected to an amplitude of a Stokes wave.

The amplitude of the nth harmonic force is made non-dimensional dividing by $\rho g A^n R^{(3-n)}$. The phase of the nth harmonic force is obtained relative to the phase of the incoming waves. The phase of the incoming waves, at a given position in the tank, changes as the wave amplitude increases, due to amplitude dispersion. The phase of the resulting force on the cylinder changes accordingly.

The typical error in the measured wave elevation is about 2%. This will introduce an error in the amplitude and phase of the non-dimensional nth harmonic force which is about n times 2%. Since the force transducers are very accurate compared to the wave gauges, we could alternatively relate the nth harmonic force components to the component of the force oscillating with the fundamental frequency. This alternative procedure is not applied in this paper.

The force measurements are compared with theoretical models. The Morison equation and the McCamy–Fuchs solution may be applied to compute the first-harmonic force. Molin (1979) and later Newman (1996*b*) have employed a second-order model for calculation of the second-harmonic wave force. Malenica & Molin (1995, hereafter referred to as M&M), have developed a third-order model using a perturbation expansion in the wave slope. A model of the third-harmonic force, using a perturbation expansion in both the wave slope and the wavenumber, has been developed by Faltinsen *et al.* (1995, hereafter referred to as FNV). Ferrant (1998) has carried out fully nonlinear computations to calculate all higher-harmonic components of the force. The incoming waves in our experiments, which are pure Stokes waves, correspond to the assumptions in the theoretical models.

For a very limited range of parameters, we also compare our measurements with experiments performed by Stansberg (1997).

While the experiments are carried out in a wave tank with a limited width b, all the theoretical models assume an unbounded horizontal fluid domain. However, with a ratio b/R from 6.3 to 8.3, we find that the limited width of the tank is not important to the investigation, except close to resonance, when standing cross-waves are generated at the cylinder. We present no results for wave parameters close to resonance.

4.1. *First-harmonic force*

To obtain an estimate of the first-harmonic force we may apply the Morison equation, giving the simple result $F_1 = 2\pi\rho g A R^2 e^{i\pi/2}$. We may also, however, calculate the complete linear exciting force by the McCamy–Fuchs solution, giving in deep water

$$F_1 = \frac{4\rho g A}{k^2 H_1^{(2)'}(kR)}, \tag{4.1}$$

where $H_1^{(2)}$ is the Hankel function of the second kind and order one, and the prime denotes differentiation. Furthermore, F_1 may be obtained from the fully nonlinear

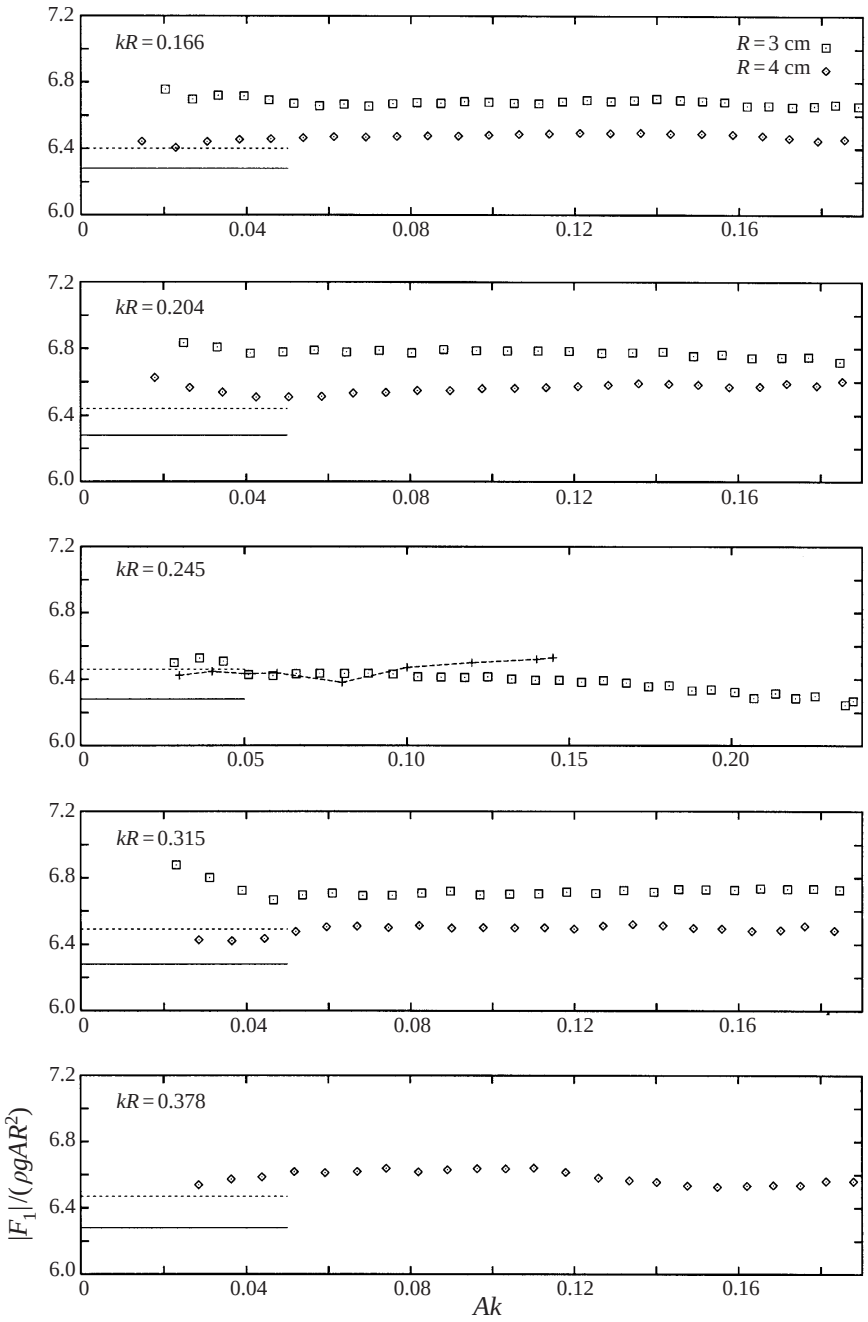

FIGURE 7. Squares and diamonds: measured amplitude of the first-harmonic force. Solid line: the Morison equation. Dashed line: the McCamy–Fuchs solution. For $kR = 0.245$ Ferrant's nonlinear computations are represented by the dashed line with crosses.

computations by Ferrant. A drag force due to the laminar boundary layer in the experiments may be estimated to be $0.1\pi\rho g A R^2$, approximately, for the two cylinders. This drag force is very small, and is not accounted for in the figures. Figure 7 shows a comparison of our measurements for the amplitude of the first-harmonic

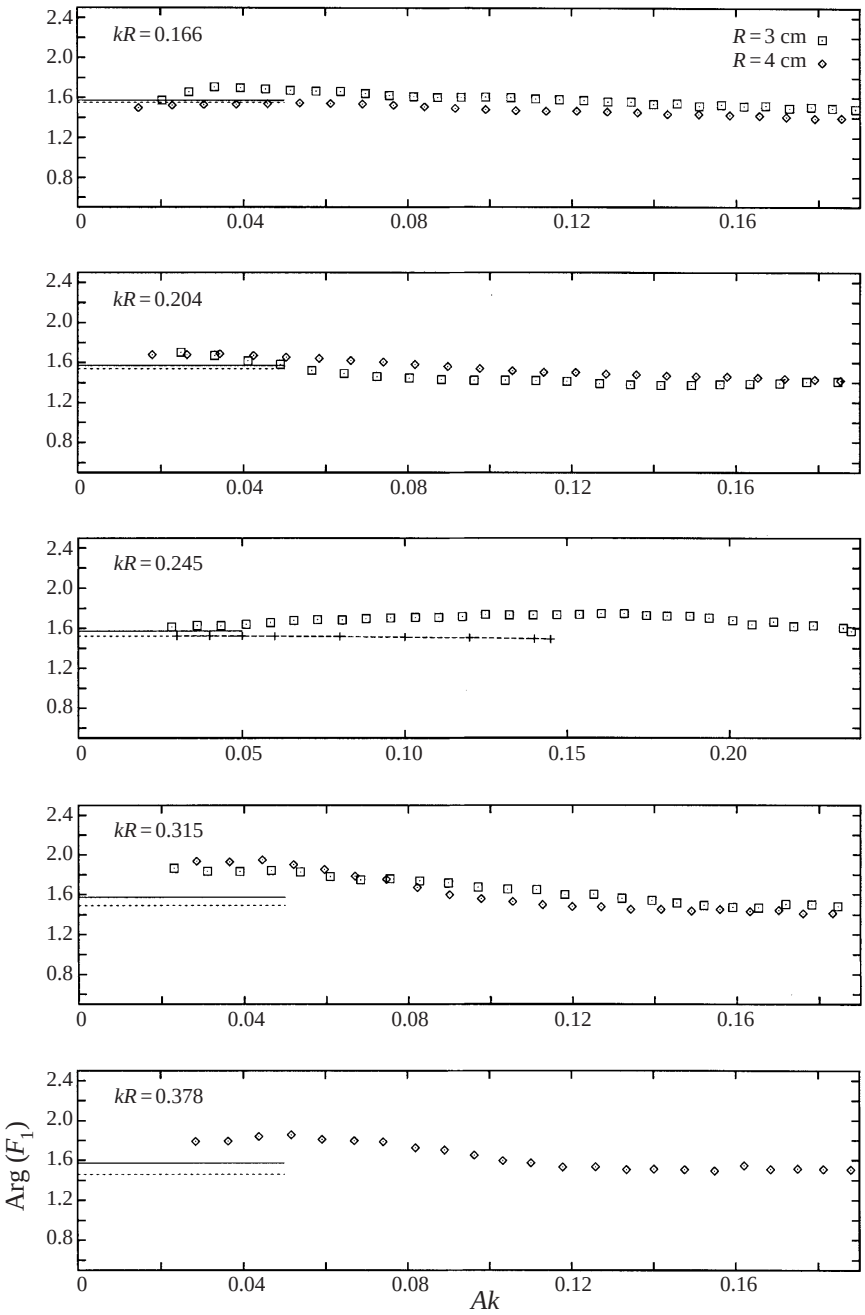

FIGURE 8. Squares and diamonds: measured phase of the first harmonic force. Straight lines represent linear models. Solid line: the Morison equation. Dashed line: the McCamy–Fuchs solution. For $kR = 0.245$ Ferrant's nonlinear computations are represented by the dashed line with crosses.

force with the model estimates, with good agreement. The phase of the first-harmonic force (figure 8) is also predicted quite well by the computations. For the two largest wavenumbers, however, the phase of the measured first-harmonic force seems to be a bit larger than predicted, for small wave slopes. We note that the amplitude and

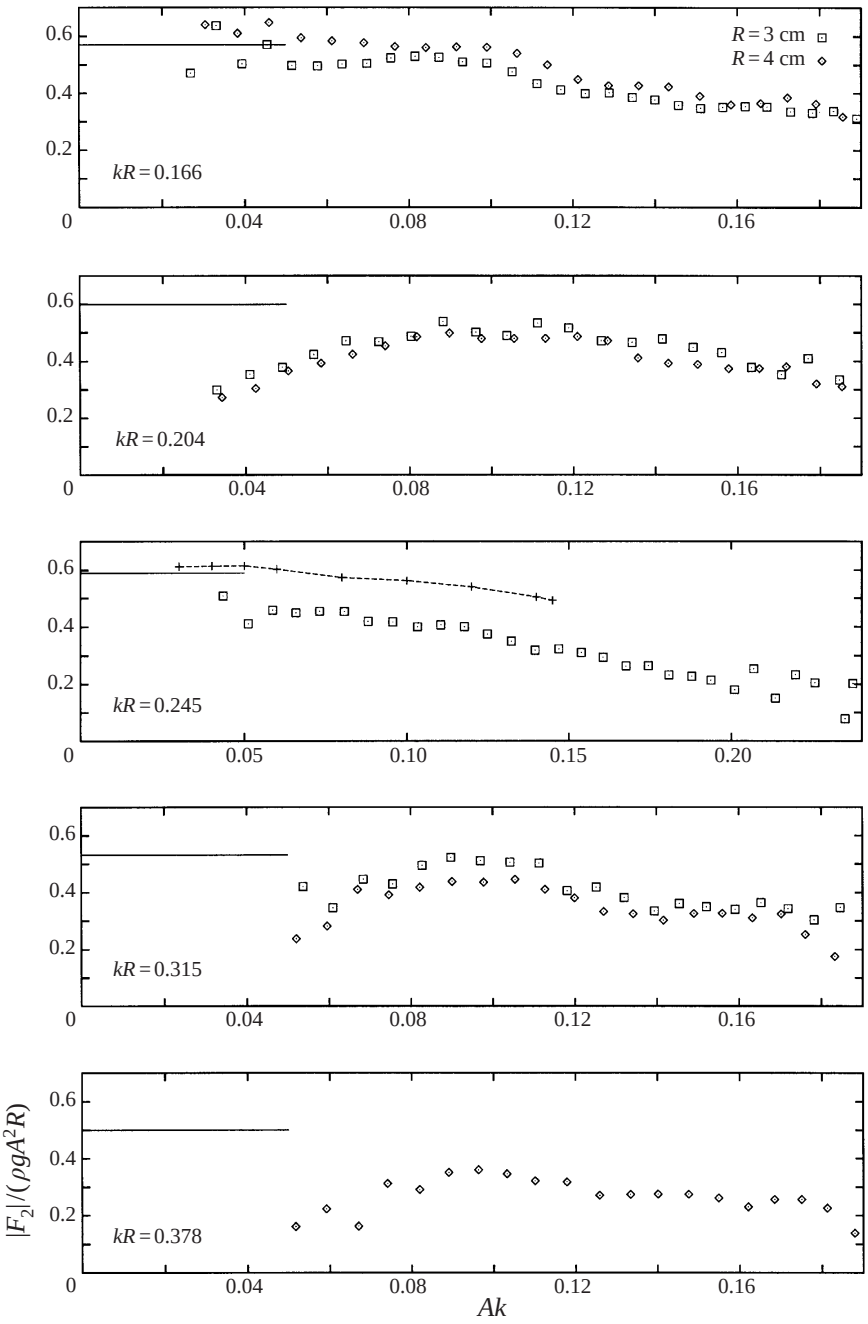

FIGURE 9. Squares and diamonds: measured amplitude of the second harmonic force. Straight line: Newman (1996*b*). For $kR = 0.245$ Ferrant's nonlinear computations are represented by the dashed line with crosses.

phase of the force are both approximately constant for the whole range of wave slopes, even when Ak has become quite large, and the expected range of validity of the perturbation models is exceeded.

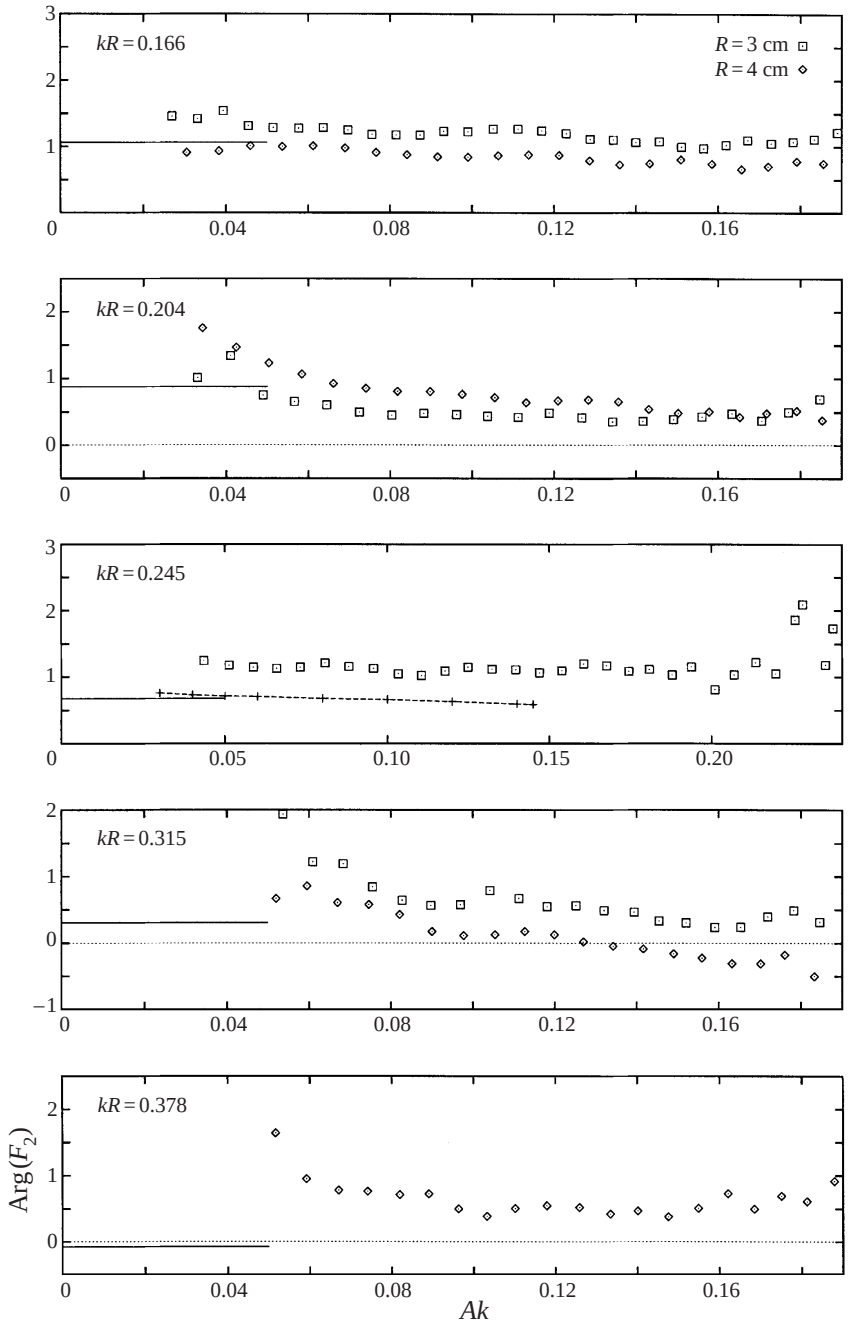

FIGURE 10. Squares and diamonds: measured phase of the second-harmonic force. Straight line: Newman (1996*b*). For $kR = 0.245$ Ferrant's nonlinear computations represented by the dashed line with crosses.

4.2. *Second-harmonic force*

For the second-harmonic force we compare our measurements with the second-order model by Molin (1979) and Newman (1996*b*) and with the fully nonlinear computations by Ferrant (1998). We observe that the amplitude of the second-

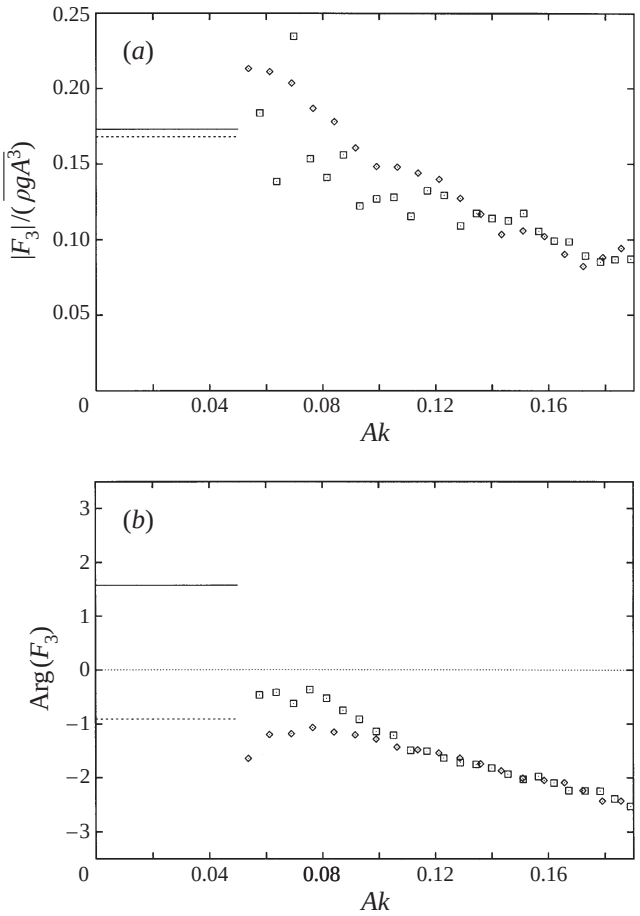

FIGURE 11. Squares ($R = 3$ cm) and diamonds ($R = 4$ cm): measurements of the amplitude and phase of the third-harmonic force with $kR = 0.166$. Straight solid line: FNV; straight dotted line: M&M.

harmonic force (figure 9) decreases as the wavenumber increases. The measured forces are smaller than the theoretical forces for all wave slopes. For large wave slopes, the measured force is significantly smaller than the theoretical results. The results by Ferrant predict the decrease of the force, observed in the experiments, though the measured force is smaller than predicted. The phase of the second-harmonic force (figure 10) is, however, quite constant as the wave slope increases, and is well predicted.

4.3. *Third-harmonic force*

For all but the smallest wavenumber, the measurements show that the amplitude of the third-harmonic force is nearly constant as the wave slope increases. There is good agreement between the measurements and the theoretical predictions of $|F_3|$ by FNV, M&M and Ferrant (figures 11–15). For the phase of F_3, the measurements agree with M&M's and Ferrant's results. We note that the FNV model provides a very simple result for the third-harmonic force, i.e. $F_3/\rho g A^3 = 2\pi(kR)^2 e^{i\pi/2}$. This model, however, predicts a value of the phase which is significantly different from our measurements. The phase predicted by FNV does not vary as a function of the wavenumber.

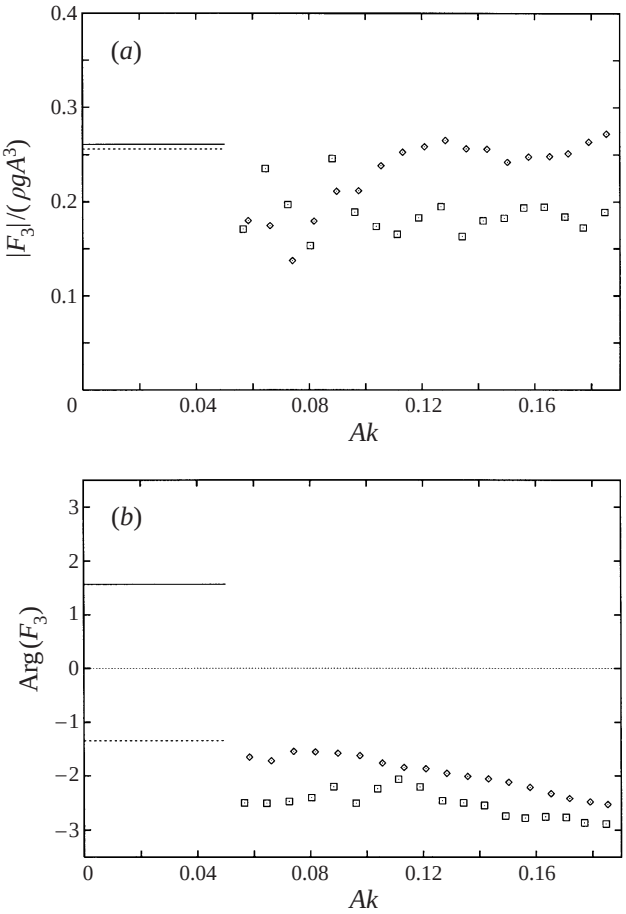

FIGURE 12. As figure 11 but with $kR = 0.204$.

We note that the third- and higher-harmonic forces are extremely small when the wave slope is small. For example, F_3 is 100 to 400 times smaller than F_1 when $Ak \approx 0.05$. This introduces difficulties in measuring and extracting the higher-harmonic components from a much larger signal. As we see in some of the figures, this causes some experimental scatter in the results, for small Ak (i.e. we have a larger relative measuring error for small Ak). Because of this we are not able to measure the third-harmonic force for wave slopes smaller than $Ak = 0.05$. Further details of how the higher-harmonic forces are extracted from the time series are given in Appendix B.

4.4. *Fourth-harmonic force*

The measurements of the fourth-harmonic force are displayed in figures 16 and 17. For one of the wavenumbers we compare with the computations by Ferrant. Because of the small size of the fourth-harmonic force, we cannot give experimental data for wave slopes less than about 0.1. We see that our measurements are in surprisingly good agreement with Ferrant's results, both for the amplitude and phase of the force. We further note that the value of $|F_4|$, to a rough approximation, behaves as $|F_4|/(\rho g A^4 R^{-1}) \sim kR$, for $kR \leqslant 0.315$ and moderate wave slope.

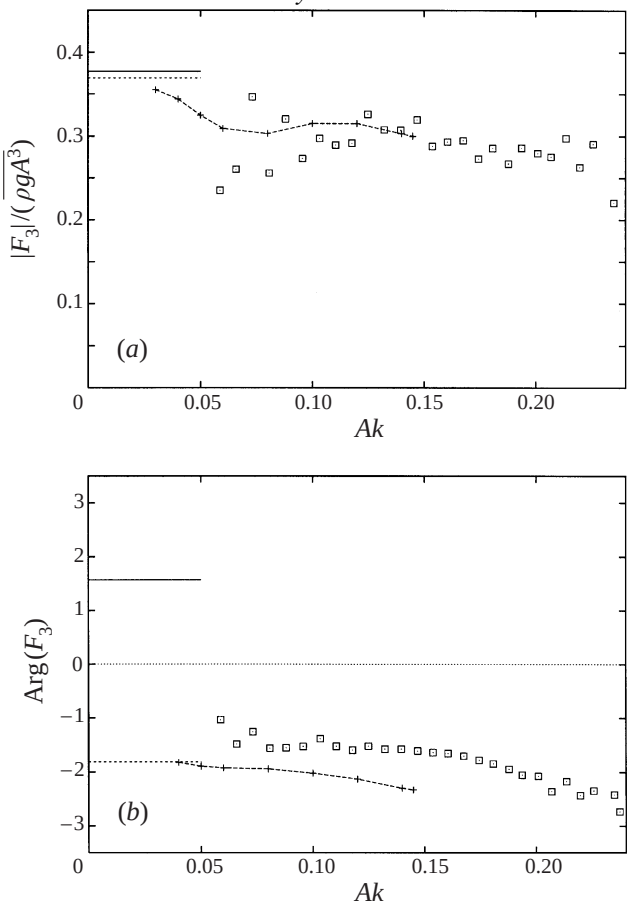

FIGURE 13. As figure 11 but for $R = 3$ cm only and $kR = 0.245$. Crossed line: nonlinear computations by Ferrant.

4.5. *Higher-harmonic forces*

We also display measurements of the amplitude and phase of the fifth-, sixth- and seventh-harmonic force components for one wavenumber ($kR = 0.245$) in figures 18–20. For these increasingly higher harmonics we require the waves to be increasingly large before we are able to measure the very small force components. We compare our measurements with the nonlinear computations by Ferrant. His results could not be obtained for wave slopes larger than $Ak = 0.145$, and our measurements for these higher harmonics could not be done for wave slopes much smaller than this. The common domain of the measurements and the calculations is thus quite small. The trend of the results, however, shows good agreement, taking into account the small size of the measured forces. The measured amplitude of the forces and theoretical results show an agreement which is well within the measurement accuracy for these extremely small forces. The measured phase of the forces is somewhat larger than predicted by theory.

4.6. *Other experiments*

Stansberg (1997) has taken measurements of the amplitude of the second- and third-harmonic force on several cylinders in periodic waves in a towing tank which is 80 m long, 10 m wide and 10 m deep. The draughts d of the cylinders were 1.44 and 0.94 m,

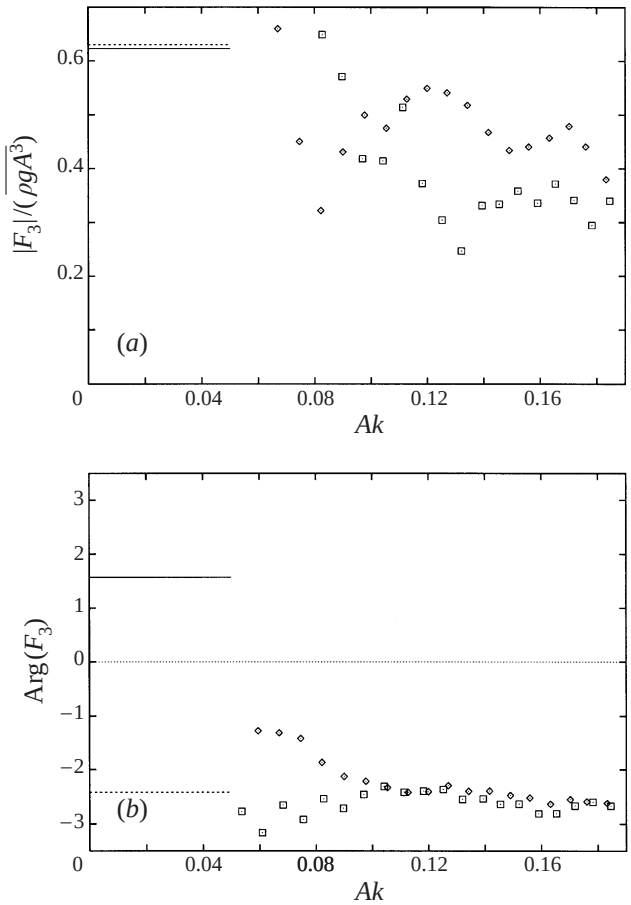

FIGURE 14. As figure 11 but with $kR = 0.315$.

and the radii 10, 16.3 and 31.3 cm. We compare our measurements with those of Stansberg where the non-dimensional wavenumber kR and draught d/R have a size relevant to our measurements, i.e. we compare our measurements with parameters $kR = 0.166$ and $d/R = 15$ or 20 ($R = 4$ cm or 3 cm) to Stansberg's measurements with parameters $kR = 0.149$ and $d/R = 8.8$ ($R = 16.3$ cm). As we see in figure 21, our measurements are in relatively good agreement with Stansberg's.

It is interesting to see that both our measurements and his give a decreasing amplitude of the third-harmonic force (figure 21*b*) for small to medium wave slopes. For Ak larger than 0.2 the measurements indicate that the amplitude of the third-harmonic force is constant.

The other results of Stansberg for d/R smaller than 8.8 show smaller values of $|F_2|$ and $|F_3|$ than obtained in our experiments. We believe that this is due to the limited draught of the cylinders in Stansberg's experiments.

5. Oscillating force and effects of viscosity

5.1. *Oscillating force*

As already mentioned, when we take measurements 12.41 m from the wave maker, we first wait for the waves to become periodic (10–15 wave periods from when the first

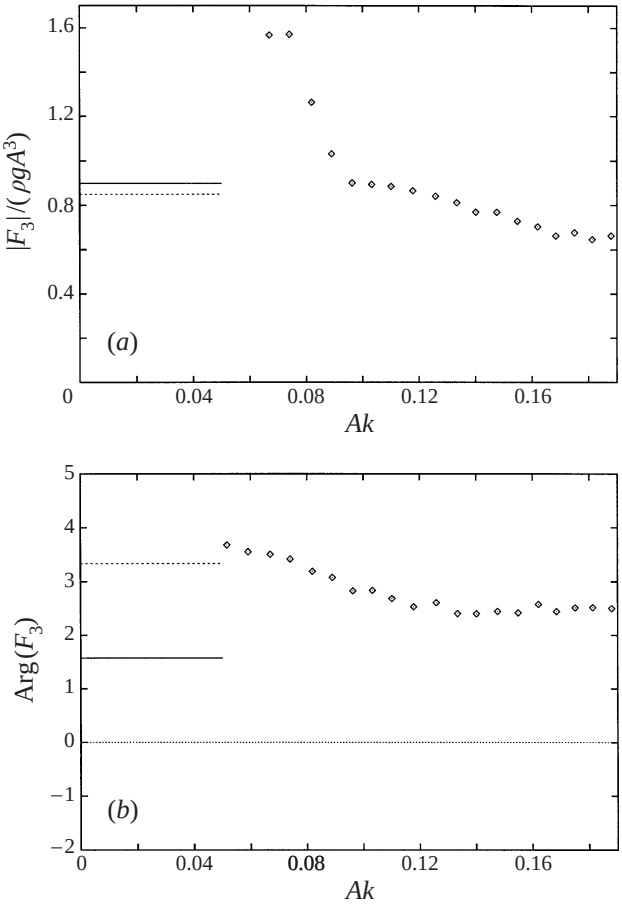

FIGURE 15. As figure 11 but for $R = 4\,\text{cm}$ only and $kR = 0.378$.

large wave has reached the cylinder). We may then take measurements over a time window of 10 wave periods before the wave field is disturbed by unwanted effects. The amplitude of e.g. the second-harmonic force will then look like that displayed in figure 22(*a*). When the force measurements are carried out in a later time window, we obtain an oscillation in the second-harmonic and higher-harmonic forces (figure 22*b*). The force oscillates around a mean value which corresponds to the force in an earlier time window (figure 22*a*). After this change of character, the measured force does not change as time increases, except for some small fluctuations which appear when the time elapsed is so long that these are reflections from the beach and the wave maker.

The same behaviour of the measured forces also occurs when the cylinder is situated at other positions in the wave tank. We have in particular investigated the higher-harmonic forces when the cylinder is placed close to the wave maker, at a distance of 6.33 m. An example for the second-harmonic force is shown in figure 23. The same oscillations, but with a smaller frequency, occur in a late time window. At this position, minor oscillations are also present in an early time window because it is impossible to find a sufficiently long time window this close to the wave maker where the incoming waves can be regarded as pure Stokes waves. Similar oscillations

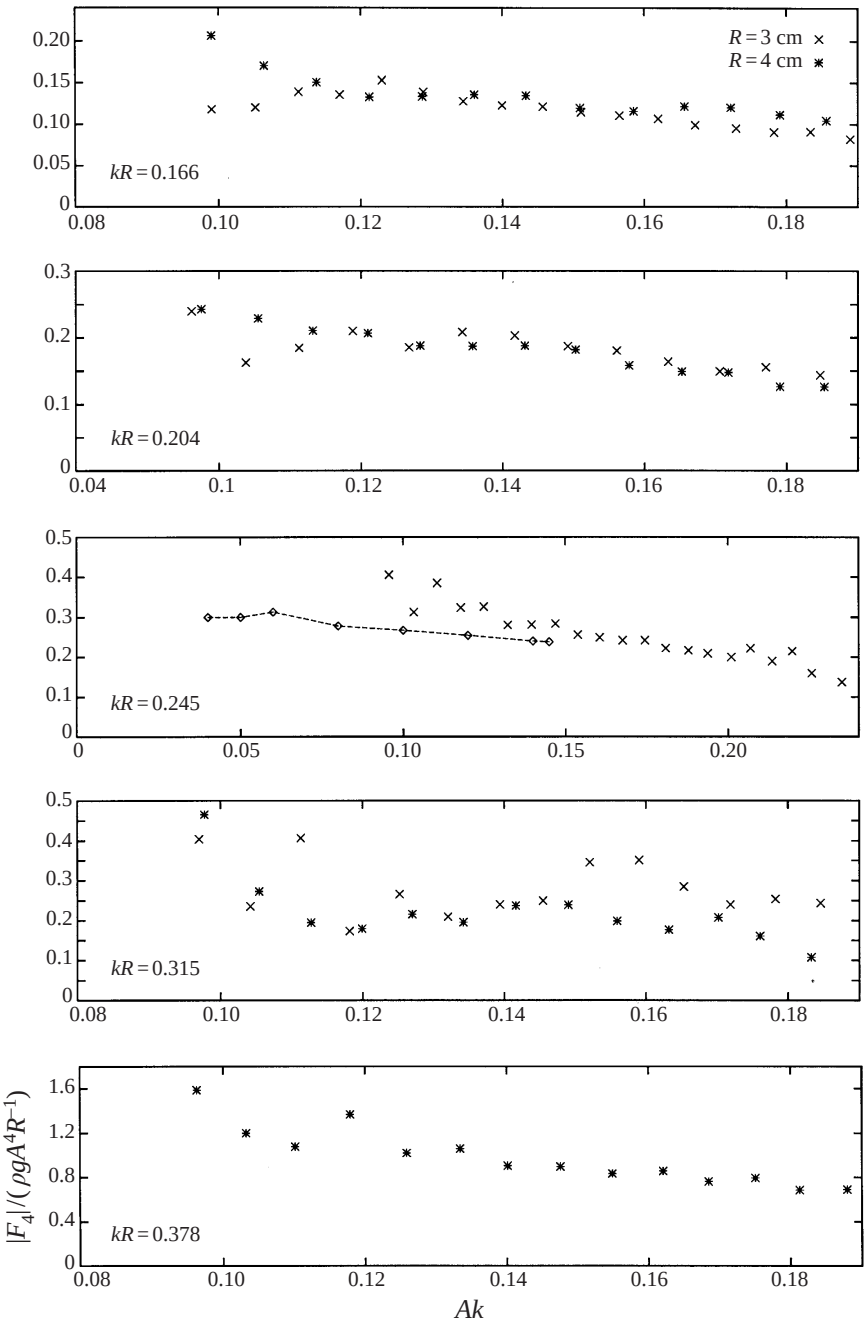

FIGURE 16. Crosses and stars: measured amplitude of the fourth-harmonic force. For $kR = 0.245$ Ferrant's nonlinear computations are represented by the dashed line with crosses.

occur also for the other higher-harmonic forces. We note that the time at which the change of character occurs in the force measurements coincides with the time when the second-harmonic parasitic waves arrive at the cylinder. This may indicate that the parasitic waves are the cause of the oscillations of the force. To document this, one would have to perform the same experiments with waves that are known

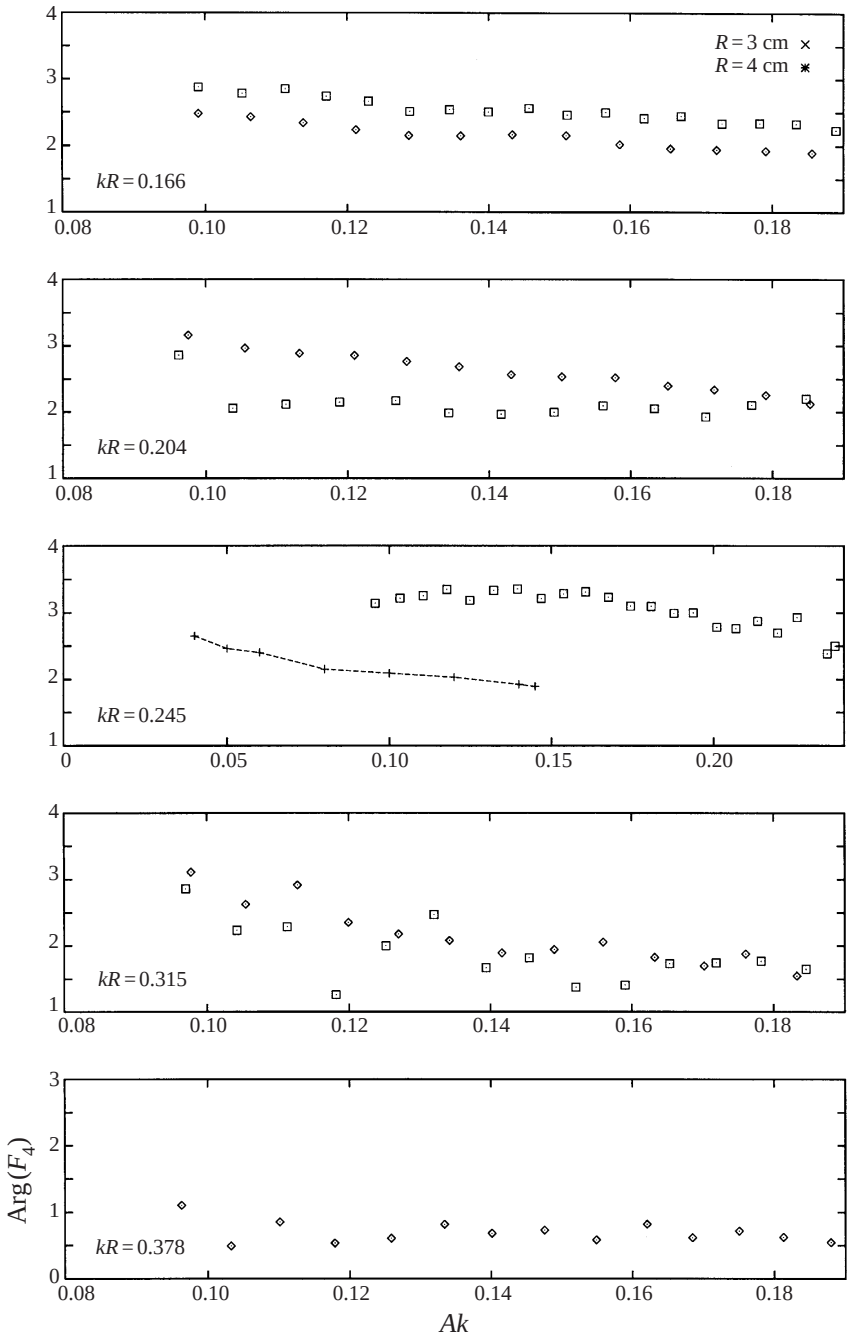

FIGURE 17. Squares and diamonds: measured phase of the fourth-harmonic force. For $kR = 0.245$ Ferrant's nonlinear computations are represented by the dashed line with crosses.

to be absolutely free from second-harmonic parasitic waves at all times. We note, however, that other nonlinear effects may lead to oscillations in the second- and higher-harmonic forces but our investigation gives no evidence on this point.

As we have seen, there exists a time window in which we can perform force

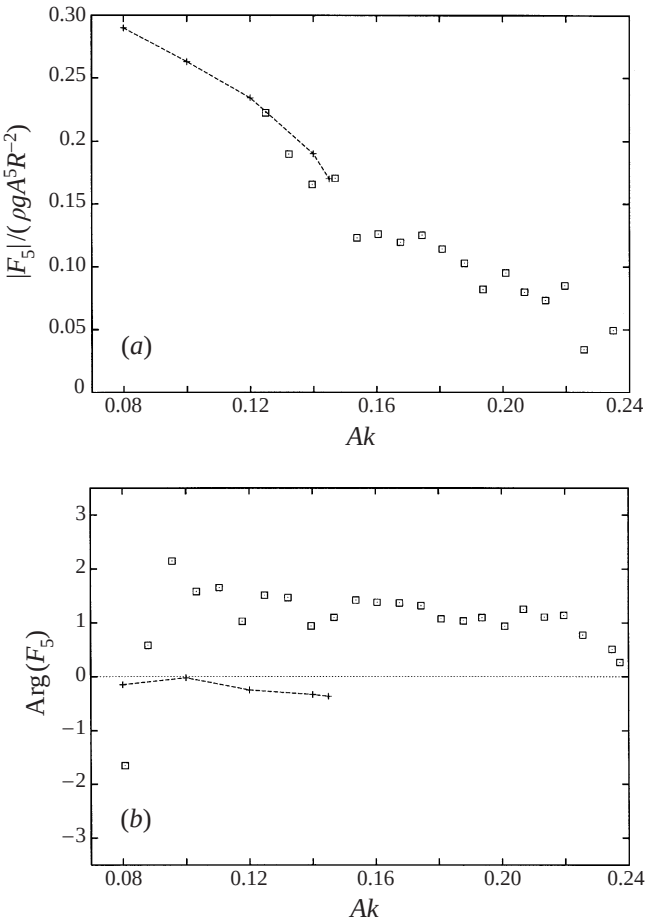

FIGURE 18. Squares: measured amplitude and phase of the fifth-harmonic force with $kR = 0.245$. Ferrant's nonlinear computations are represented by the dashed line with crosses.

measurements without getting oscillations in the force as the wave slope increases. The length of this time window will be proportional to the distance from the wave maker to the cylinder. Too close to the wave maker, there is no time window of sufficient length where we can assume that the incoming wave field is pure Stokes waves and thus we will expect to always get oscillations in the force measurements here. In our experiments, we required a distance of at least 10 wavelengths from the wave maker to the cylinder.

All of the measurements of the force that are presented in the previous section are conducted 12.41 m or 15.45 m from the wave maker. We were then able to use a suitable time window, so that the problems discussed in this section do not relate to the force measurements presented here.

5.2. *Viscous effects*

When the wave height is large compared to the cylinder diameter, the values of the Keulegan–Carpenter number KC and the Reynolds number Re become important parameters in the problem. In the present experiments $1 < KC < 3.6$, and $Re \sim 20\,000$, for the large waves. Sarpkaya (1986, figure 3) shows that the viscous drag force on a circular cylinder is very small for these values of KC and Re. Here we

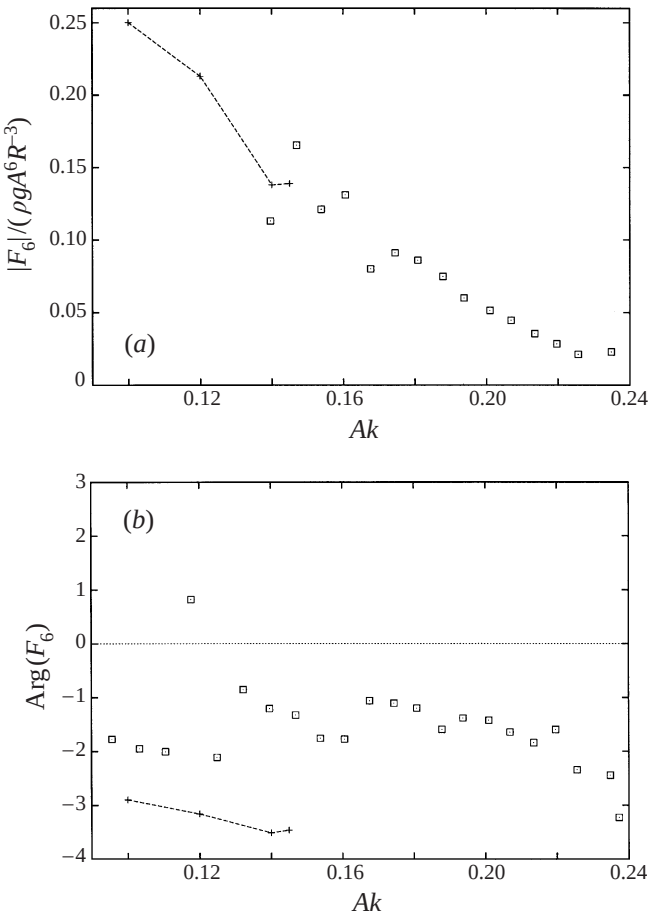

FIGURE 19. Squares: measured amplitude and phase of the sixth-harmonic force with $kR = 0.245$. Ferrant's nonlinear computations are represented by the dashed line with crosses.

have estimated the drag force to have a magnitude of $0.1\pi\rho g A R^2$. We also note that we have not observed flow separation in the experiments.

6. Conclusion

We have performed an extensive set of experiments with a vertical circular cylinder in periodic waves. The purpose has been to measure the first- and higher-harmonic horizontal wave loads on the cylinder. We have also performed an extensive set of measurements of the incoming waves, without the cylinder present, to document that the wave field is of pure Stokes waves in a relatively long time window. This is true for waves with wave slope up to about 0.2. For larger wave slope, the incoming wave field contains disturbances in addition to the Stokes waves. We found that the (periodic) Stokes waves are present in a relatively early, but relatively long time window, at the selected measurement positions. In a later time window, second-harmonic parasitic waves appear, originating from the wave maker. Our recordings of these waves agree with previous results by e.g. Schäffer (1996). Parasitic waves become present very early when the recording position is close to the wave maker.

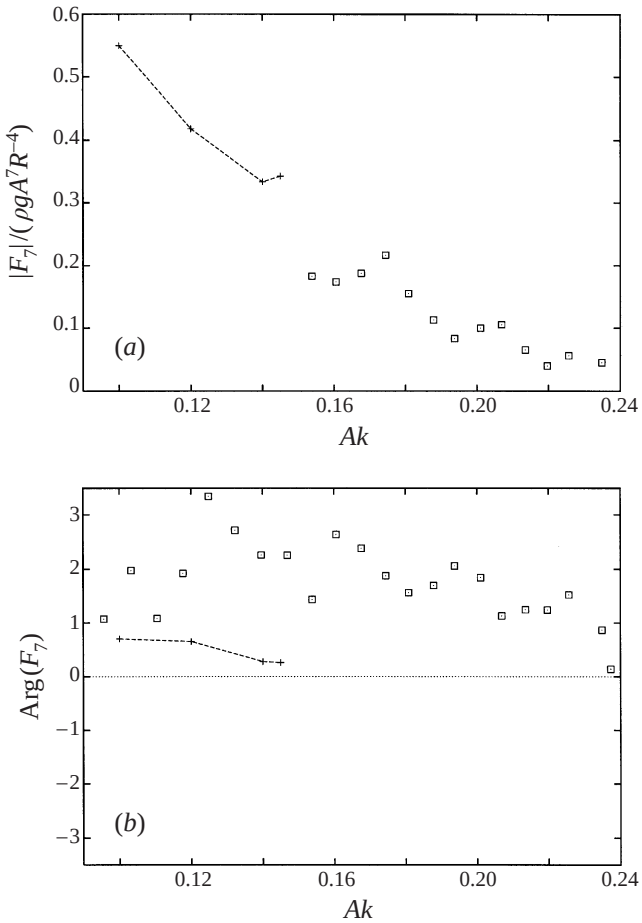

FIGURE 20. Squares: measured/amplitude and phase of the seventh-harmonic force with $kR = 0.245$. Ferrant's nonlinear computations are represented by the dashed line with crosses.

Experiments with two cylinders of different radii have been undertaken. The larger cylinder is placed further from the wave maker than the smaller one, such that the distance relative to the cylinder radius is the same. The waves are also correspondingly longer for the larger cylinder than for the smaller, so that the waves travel the same number of wavelengths down the wave tank before they reach the cylinders. The only difference between the experiments on the two different cylinders is the ratio of the tank width to the radius of the cylinder, which is 6.3 for the larger cylinder and 8.3 for the smaller one. The results indicate that the limited width of the wave tank is not important to the investigation, except close to resonance, where results are not given, however. This is also confirmed by the comparisons with the theoretical models, where the models assume a fluid which is unbounded horizontally. We have, on the other hand, found that it is important to perform the measurements with the cylinder at a sufficiently large distance from the wave maker, to avoid misleading results. In our experiments the distance to the wave maker is more than ten wavelengths.

The nth harmonic force is made non-dimensional with respect to $\rho g A^n R^{3-n}$, and its phase is measured relative to the phase of the incoming waves. The measured complex non-dimensional first-harmonic force is found to be approximately constant

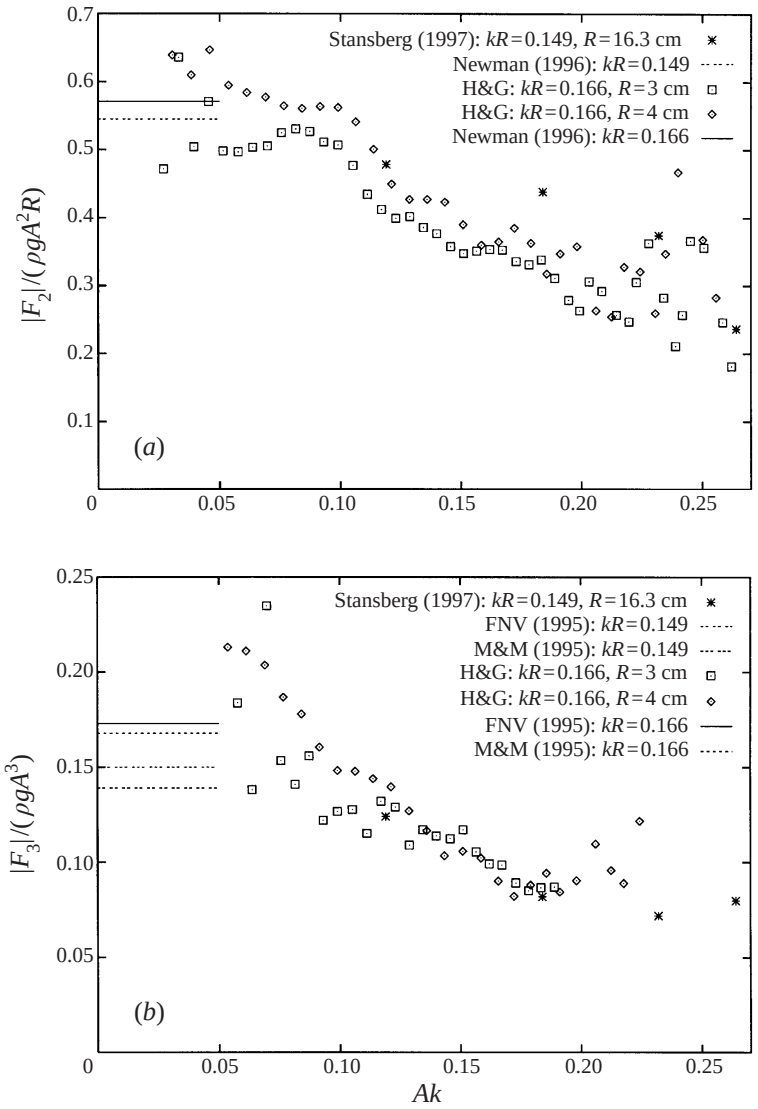

FIGURE 21. Comparison between measurements by Stansberg (1997) and our measurements (H&G). The straight lines represent theoretical models. (*a*) Amplitude of the second-harmonic force. (*b*) Amplitude of the third-harmonic force.

for all wave slopes investigated, i.e. for Ak up to about 0.2. We find that the first-harmonic force is rather well predicted by the Morison equation or alternatively the McCamy–Fuchs solution. The non-dimensional second-harmonic force is always less than 10% of the non-dimensional first-harmonic force. Second-order models (Molin 1979; Newman 1996*b*) are found to be in reasonable agreement with the measurements for most of the wavenumbers, for small and moderate wave slope. The second-harmonic force decreases with increasing wave slope and becomes significantly smaller than predicted by the second-order models when Ak is around 0.2. The phase of the second-harmonic force is reasonably constant as function of the wave amplitude and is in good agreement with the second-order models for all wavenumbers.

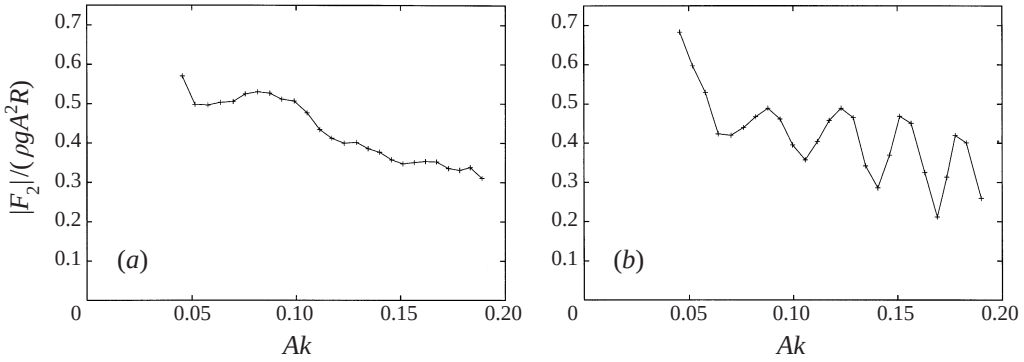

FIGURE 22. Measurements of the second-harmonic force with $kR = 0.166$ for the $R = 3$ cm cylinder. The distance from the cylinder to the wave maker is 12.41 m. Early time window. (*a*) Late time window.

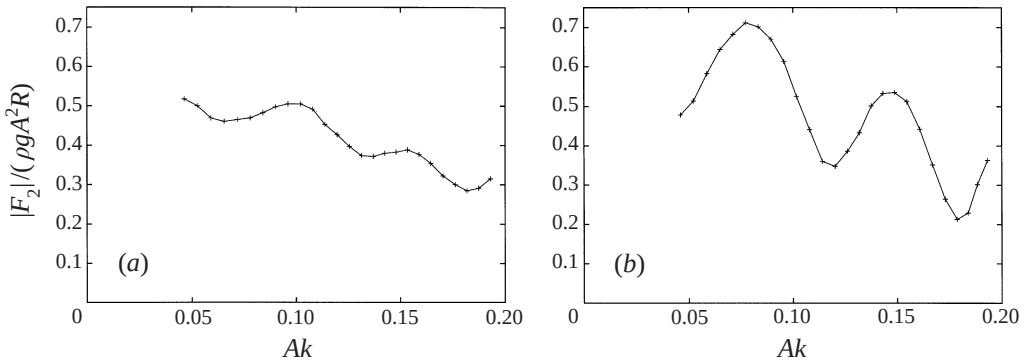

FIGURE 23. As figure 22 but the distance from the cylinder to the wave maker is 6.33 m.

The measured third-harmonic force has a magnitude which agrees rather well with M&M who assume a Stokes perturbation expansion, and with FNV who use an asymptotic approach assuming $Ak \ll 1$, $kR \ll 1$ and $A/R = O(1)$. This is true for all investigated wavenumbers when the wave slope is small or moderate. The measured $|F_3|$ is somewhat smaller than predicted by the above models when the wave slope is large, however. The measured phase of F_3 is in good agreement with the model by M&M, for all wavenumbers, but differs significantly from the predictions by the FNV model. Our results for the amplitude of the second- and third-harmonic forces are found to compare well with a set of the measurements performed by Stansberg (1997), for cylinders of larger scale in a wider wave tank than ours.

The measured fourth-harmonic force has an amplitude which to a rough approximation behaves as $|F_4|/(\rho g A^4 R^{-1}) \sim kR$ when $kR < 0.315$. This force component has a different behaviour when the wavenumber is larger than 0.315, however. We find that the phase of the fourth-harmonic force varies with respect to the wavenumber, but is relatively constant as function of the wave slope, like for the lower-harmonic forces. We also present measurements of the fifth-, sixth- and seventh-harmonic forces on the cylinders when the wavenumber is $kR = 0.245$. The magnitude of these (non-dimensional) forces exhibits a pronounced decay with increasing amplitude and becomes very small when Ak is larger than 0.2. The phases of these forces are relatively constant in the whole wave amplitude range. From the few comparisons we

have carried out, it seems that the nonlinear computations by Ferrant (1998) predict the measured higher-harmonic forces well, in a limited wave amplitude range. It would be interesting to know if this or other nonlinear methods can predict the other measured results that are included in this investigation.

For three of the wavenumbers, the measurements are carried out with incoming wave amplitude increasing up to the radius of the cylinder. At this value of the wave amplitude, the second-, third- and fourth-harmonic forces all become of equal size. The fifth-, sixth- and seventh-harmonic forces are, however, always smaller than the lower harmonics.

We finally note some observations from the experiments additional to those already described. In the early part of the force histories, where the incoming waves are not yet periodic, rather intense higher harmonic forces may occur when the wave elevation is sufficiently large. These higher-harmonic forces seem to be much more pronounced than those due to incoming Stokes waves. The problem of higher-harmonic wave loads in transient wave trains, leading to ringing, is currently under investigation in the Hydrodynamic Laboratory at the University of Oslo.

The authors are grateful to Dr Pierre Ferrant for exchange of scientific results and to Mr Arve Kvalheim and Mr Svein Vesterby for their skillful technical assistance. This work was supported by the Joint Industry Project Deep Water Analysis Tools – 'DEEPER'. We are grateful for the support of the individual sponsors, including The Research Council of Norway, Norsk Hydro, Statoil, Saga Petroleum, Mobil, Petrobras, Aker Engineering, Kvaerner Oil & Gas, Offshore Design, Brown & Root, J. Ray McDermott, Umoe Technology, ETPM SA, AMECRC and Det Norske Veritas.

Appendix A. Instabilities from the set-up

The input to the wave maker is a pure sinusoidal movement. Depending on the precision of the equipment that is used to move the wave maker, a narrow side band will be introduced in the amplitude spectrum of the movement of the wave maker, and thereby a narrow side band in the amplitude spectrum of the wave elevation. In our experiments this possible side band in the wave elevation is so narrow that we cannot measure it using a discrete Fourier transform over 10 wave periods. It would however appear at some point, as a modulation, if the wave tank was long enough for the waves to keep on propagating. The extent to which this side band gives rise to instabilities will depend on the distance from the wave maker to the measuring position, the breadth of the tank, the frequency of the waves, the accuracy of the equipment that controls the wave maker and the precision of the wave tank (i.e. if the walls of the wave tank are completely parallel). We have not observed side band instabilities in the present experiments.

Appendix B. Some aspects of Fourier analysis of periodic signals

When analysing the measurements in this paper, we typically want to extract a small higher-harmonic signal from a large signal, which is assumed to be periodic. Typically the third harmonic can be from 10 to 400 times smaller than the first harmonic. It is thus difficult to obtain the higher harmonics with high accuracy.

We will consider here some aspects of performing a Fourier analysis on a periodic signal. The continuous function $f(t) = a_1 \cos(\Omega_1 t) + a_2 \cos(2\Omega_1 t)$ is used as an example.

Here t is time, Ω_1 is the first-harmonic (or fundamental) angular frequency of the signal, and a_1 and a_2 are the size of the first and second harmonic, respectively.

If we sample this continuous signal N times, with a sampling rate of f_s (i.e. $t = n/f_s$), we get the sequence

$$f[n] = a_1 \cos[\omega_1 n] + a_2 \cos[2\omega_1 n], \tag{B 1}$$

where the integer n is the index of the sequences and $\omega_1 = \Omega_1/f_s$.

The Fourier transform (FT) $F(\omega)$ of this discrete sequence of length N, and the corresponding synthesis equation are

$$F(\omega) = \sum_{n=0}^{N-1} f[n] \mathrm{e}^{-\mathrm{i}n\omega}, \qquad f[n] = \frac{1}{2\pi} \int_{-\pi}^{\pi} F(\omega) \mathrm{e}^{\mathrm{i}n\omega} \, \mathrm{d}\omega. \tag{B 2}$$

Note that the FT is periodic in ω with period of 2π, and that the frequency $\omega = \pi$ corresponds to the continuous time frequency $\Omega = 1/2f_s$, i.e. the Nyquist frequency. We also note that the first two components of a Fourier series with fundamental frequency ω_α can be found using

$$A_1 = \frac{2}{N}|F(\omega_\alpha)| \qquad A_2 = \frac{2}{N}|F(2\omega_\alpha)|, \tag{B 3}$$

where A_1 and A_2 are the harmonic components resulting from the Fourier analysis. It is, however, a_1 and a_2 that represent the actual size of the harmonic components of the signal. We aim to show that a small discrepancy between the assumed frequency ω_α and the actual frequency ω_1, may lead to a large discrepancy between A_2 and a_2 if a_1/a_2 is large.

If we let N (and hence time) approach infinity, we may write

$$\begin{aligned} \tilde{F}(\omega) = \lim_{N\to\infty} F(\omega) = \pi \sum_{k=-\infty}^{\infty} (a_1 \delta(\omega - \omega_1 + 2\pi k) + a_2 \delta(\omega - 2\omega_1 + 2\pi k) \\ + a_1 \delta(\omega + \omega_1 + 2\pi k) + a_2 \delta(\omega + 2\omega_1 + 2\pi k)), \end{aligned} \tag{B 4}$$

where $\delta(\omega)$ is the Dirac delta function. Even though the FT of a periodic infinite-length signal is not summable, the result in (B 4) is provided by the theory of generalized functions (Lighthill 1958), and is in common use in the field of time-discrete signal processing.

Using the windowing theorem (e.g. Oppenheim & Schafer 1989), we can then show that the FT of the time-limited sequence may be written as the periodic convolution

$$F(\omega) = \frac{1}{2\pi} \int_{-\pi}^{\pi} \tilde{F}(\omega_d) W(\omega - \omega_d) \, \mathrm{d}\omega_d, \tag{B 5}$$

where $W(\omega)$ is the FT of the windowing function ($w[n] = 1$ for $n \in [0, N-1]$ and 0 elsewhere) and has the form

$$W(\omega) = \sum_{n=0}^{N-1} \mathrm{e}^{-\mathrm{i}\omega n} = \mathrm{e}^{-\mathrm{i}(\omega/2)(N-1)} \frac{\sin(\frac{1}{2}\omega N)}{\sin(\frac{1}{2}\omega)}. \tag{B 6}$$

Note that $W(0) = N$, and that $W(\omega)$ is periodic in ω with period 2π.

Substituting (B 4) into (B 5) and calculating the integral gives the following expression for the FT (see also figure 24):

$$F(\omega) = \frac{a_1}{2} W(\omega - \omega_1) + \frac{a_2}{2} W(\omega - 2\omega_1) + \frac{a_1}{2} W(\omega + \omega_1) + \frac{a_2}{2} W(\omega + 2\omega_1). \tag{B 7}$$

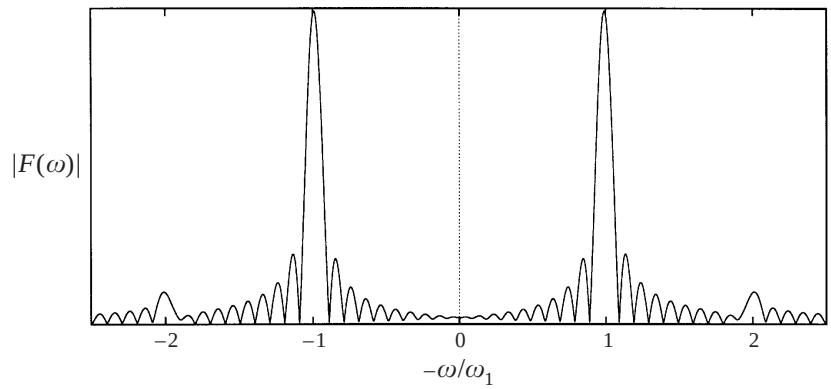

FIGURE 24. The FT of 10 wave periods, with $a_1/a_2 = 10$, $\Omega = 2 \times 1.25$.

We now chose N so that the sampled sequence consists of precisely 10 periods of the fundamental oscillation, i.e. $N = 10(2\pi/\Omega_1)f_s$. Then $\omega_1 = 10(2\pi/N)$. From (B 3), (B 6) and (B 7) we have

$$A_2 = \frac{2}{N}|F(2\omega_1)| = \frac{2}{N}|\frac{a_1}{2}W(\omega_1) + \frac{a_2}{2}W(0) + \frac{a_1}{2}W(3\omega_1) + \frac{a_2}{2}W(4\omega_1)| = a_2. \quad \text{(B 8)}$$

We see that the second-harmonic component of the FT, A_2, is equal to a_2.

If we, however, assume that the fundamental frequency of the periodic signal is a little different from ω_1, we may have that $A_2 \neq a_2$. Assuming the fundamental frequency of the signal to be $\omega_\alpha = (1+\epsilon)\omega_1$ (ϵ is a small number), we will sample $N = 10(2\pi/\Omega_\alpha)f_s$ points from the continuous signal. The main difference from the previous case is that the width of the side lobes of $W(\omega)$ change. The second-harmonic component of the FT will then be

$$|F(2\omega_\alpha)| = |\frac{a_1}{2}W((1+2\epsilon)\omega_1) + \frac{a_2}{2}W(2\epsilon\omega_1) + \frac{a_1}{2}W((3+2\epsilon)\omega_1) + \frac{a_2}{2}W((4+2\epsilon)\omega_1)|. \quad \text{(B 9)}$$

As an example, setting $\Omega_1 = 2\pi \times 1.25$, $a_1/a_2 = 50$ and $\epsilon = 0.01$ (i.e. we have estimated the frequency of the signal wrongly by 1%), we obtain $A_2 = (2/N)|F(2\omega_\alpha)| = 1.31a_2$.

Thus we see that in this example an error of 1% in the estimate of the fundamental frequency of the signal gives an error in the second-harmonic amplitude of 31%. The largest part of this error comes from the first term on the right of (B 9). The reason for this is, as we have seen, that the width of the side lobes of the FT of the windowing function is such that the first-harmonic component interferes with the higher-harmonic component.

In our measurements, we believe that we have very good control of the frequency of the waves. The results will however always be affected by the inconsistency between the assumed frequency and the actual frequency, for instance caused by the need for truncation of the frequency as a result of the finite number of sampling points. We believe that it is important to understand the accuracy of Fourier analysis of small higher-harmonic signals to be able to interpret the results correctly.

REFERENCES

CAI, X. & MELUM, E. 1996 Two fragments of a method for fully nonlinear simulation of water waves. In *Waves and Nonlinear Processes in Hydrodynamics* (ed. J. Grue, B. Gjevik & J. E. Weber), pp. 37–50. Kluwer.

CHAPLIN, J. R., RAINEY, R. C. T. & YEMM, R. W. 1997 Ringing of a vertical cylinder in waves. *J. Fluid Mech.* **350**, 119–147.

FALTINSEN, O. M., NEWMAN, J. N. & VINJE, T. 1995 Nonlinear wave loads on a slender vertical cylinder. *J. Fluid Mech.* **289**, 179–199 (referred to herein as FNV).

FERRANT, P. 1998 Fully non linear interactions of long-crested wave packets with a three dimensional body. *22nd ONR Symposium in Naval Hydrodynamics, Washington D.C.* Tuesday/Wednesday Sessions Provisional Proceedings, pp. 59–72.

GRUE, J. 1992 The nonlinear water waves at a submerged obstacle or bottom topography. *J. Fluid Mech.* **244**, 455–476.

GRUE, J., BJØRSHOL, G. & STRAND, Ø. 1993 Higher harmonic wave exciting forces on a vertical cylinder. *Institute of Mathematics, University of Oslo Preprint* 2. ISBN 82-553-0862-8.

LIGHTHILL, M. J. 1958 *Introduction to Fourier Analysis and Generalized Functions.* Cambridge University Press.

MALENICA, S. & MOLIN, B. 1995 Third-harmonic wave diffraction by a vertical cylinder. *J. Fluid Mech.* **302**, 203–229 (referred to herein as M&M).

MOLIN, B. 1979 Second-order diffraction loads upon three dimensional bodies. *Appl. Ocean Res.* **1**, 197–202.

NEWMAN, J. N. 1996*a* Nonlinear scattering of long waves by a vertical cylinder. In *Waves and Nonlinear Processes in Hydrodynamics* (ed. J. Grue, B. Gjevik & J. E. Weber), pp. 91–102. Kluwer.

NEWMAN, J. N. 1996*b* The second-order wave force on a vertical cylinder. *J. Fluid Mech.* **320**, 417–443.

OPPENHEIM, A. V. & SCHAFER, R. W. 1989 *Discrete Time Signal Processing*. Prentice-Hall.

SARPKAYA, T. 1986 Force on a circular cylinder in viscous oscillatory flow at low Keulegan-Carpenter numbers. *J. Fluid Mech.* **165**, 61–71.

SCHÄFFER, H. A. 1996 Second-order wave maker theory for irregular waves. *Ocean Engng* **23** 1, 47–88.

STANSBERG, C. T. 1997 Comparing ringing loads from experiments with cylinders of different diameters - An empirical study. *Proc. 8th Conf. on the Behaviour of Offshore Structures (BOSS'97)*, Vol. 2, pp. 95–109. Pergamon/Elsevier.

STANSBERG, C. T., HUSE, E., KROKSTAD, J. R. & LEHN, E. 1995 Experimental study of nonlinear loads on vertical cylinders in steep random waves. *Proc. 5th ISOPE Conf.*, Vol. I, pp. 75–82. ISOPE, Golden, Colorado, USA.